

# Nonsingular Bianchi type I cosmological solutions from the 1-loop superstring effective action

Shinsuke Kawai\*

*Graduate School of Human and Environmental Studies, Kyoto University, Kyoto 606-8501, Japan*

Jiro Soda†

*Department of Fundamental Sciences, FIHS, Kyoto University, Kyoto 606-8501, Japan*

(Received 20 July 1998; published 17 February 1999)

Nonsingular Bianchi type I solutions are found from the effective action with a superstring-motivated Gauss-Bonnet term. These anisotropic nonsingular solutions evolve from the asymptotic Minkowski region, subsequently superinflate, and then smoothly continue either to Kasner-type (expanding in two directions and shrinking in one direction) or to Friedmann-type (expanding in all directions) solutions. We also find a new kind of singularity which arises from the fact that the anisotropic expansion rates are a multiple-valued function of time. The initial singularity in the isotropic limit of this model belongs to this new kind of singularity. In our analysis the anisotropic solutions are likely to be singular when the superinflation is steep. As for the cosmic no-hair conjecture, our results suggest that the kinetic-driven superinflation of our model does not isotropize the space-time. [S0556-2821(99)02106-2]

PACS number(s): 98.80.Hw, 04.20.Dw, 04.50.+h, 11.25.Mj

## I. INTRODUCTION

Stimulated by the developments of superstring theory, various cosmological solutions based on string theory have been proposed. Although the theory has not developed enough to present a unique history of our universe in its earliest stage, one may now imagine that the big bang is no longer just a point of enigma named the initial singularity but has a rich and complex structure.

Among these string-based universe models, the most widely studied would be the so-called pre-big-bang model [1] (in the literature it is often called string cosmology). The remarkable aspect of this model is that it tries to explain the inflationary behavior of the early universe by introducing a polelike acceleration phase (superinflation) which is driven by the kinetic term of the dilaton. This superinflationary branch of the solution has a dual relation named the scale factor duality with the Friedmann branch, which is the usual decelerating expansion of the universe. The biggest problem arising in the pre-big-bang model is the difficulty of connecting the superinflationary branch and the Friedmann branch (termed the graceful exit problem), and there are no-go theorems proved under some assumptions [2].

Antoniadis, Rizos, and Tamvakis [3] proposed a nonsingular (i.e., free of the graceful exit problem) cosmological model by including the 1-loop (genus) correction term in the low-energy string effective action. This 1-loop model is excellent in that it gives a simple example of the smooth transition between the superinflationary branch and the Friedmann branch. This original 1-loop model involves dilaton and modulus fields, and there is a simplified version [4] by Rizos and Tamvakis with a modulus field only. This metric-modulus system gives essentially the same nonsingular solution as the full metric-dilaton-modulus system, since the be-

havior of the solution mainly depends only on the modulus field. The existence of the nonsingular solution is analytically shown by Rizos and Tamvakis [4] for the Friedmann-Robertson-Walker (FRW) metric, i.e., assuming the homogeneity and isotropy of the universe. We studied whether the nature of this nonsingular solution is affected if anisotropy is included. The purpose of this paper is to extend the solution of this metric-modulus system to include anisotropy and to observe the behavior of its solutions, particularly of nonsingular ones.

The following sections of this paper are organized as follows. In Sec. II we briefly review the isotropic case studied by Rizos and Tamvakis [4], and then derive the basic equations of motion from the effective action for the Bianchi type I metric. We also solve these equations analytically in the asymptotic region. In Sec. III we solve these equations numerically. We study the solutions through several cross sections of the parameter space. The existence of nonsingular anisotropic solutions is shown, and the nature of the singularity is also examined. Implications of our results are discussed in the last section.

## II. MODEL AND EQUATIONS OF MOTION

We start with the action<sup>1</sup> given by [4]

$$S = \int d^4x \sqrt{-g} \left\{ \frac{1}{2} R - \frac{1}{2} (D\sigma)^2 - \frac{\lambda}{16} \xi(\sigma) R_{GB}^2 \right\}, \quad (1)$$

<sup>1</sup>This action is also justifiable in more solid grounds. In the  $N = 4$  superstring compactifications (heterotic on  $T^6$  or type IIA on  $K3 \times T^2$ ) the function  $\xi(\sigma)$  given in Eq. (3) describes the exact  $R^2$  couplings including nonperturbative effects [6]. These vacua exhibit an exact  $S$  duality, which is identical with the  $SL(2, Z)$  modular invariance on  $\sigma$ .

\*E-mail address: kawai@phys.h.kyoto-u.ac.jp

†E-mail address: jiro@phys.h.kyoto-u.ac.jp

which is essentially the same as the 1-loop-corrected 4-dimensional effective action of orbifold-compactified heterotic string [3],

$$S = \int d^4x \sqrt{-g} \left\{ \frac{1}{2} R - \frac{1}{4} (D\Phi)^2 - \frac{3}{4} (D\sigma)^2 + \frac{1}{16} [\lambda_1 e^\Phi - \lambda_2 \xi(\sigma)] R_{GB}^2 \right\}, \quad (2)$$

except that the dilaton field  $\Phi$  is neglected.  $R$ ,  $\Phi$  and  $\sigma$  are the Ricci scalar curvature, the dilaton, and the modulus field, respectively. Our convention is  $g_{\mu\nu} = (-, +, +, +)$ ,  $R^\mu{}_{\alpha\nu\beta} = \Gamma^\mu{}_{\alpha\beta,\nu} + \dots$ ,  $R_{\alpha\beta} = R^\mu{}_{\alpha\mu\beta}$ , and  $8\pi G = 1$ . The Gauss-Bonnet curvature is defined as  $R_{GB}^2 = R^{\mu\nu\kappa\lambda} R_{\mu\nu\kappa\lambda} - 4R^{\mu\nu} R_{\mu\nu} + R^2$ , and  $\xi(\sigma)$  is a function determining the coupling of  $\sigma$  and the geometry, written in terms of the Dedekind  $\eta$  function as

$$\begin{aligned} \xi(\sigma) &= -\ln[2e^\sigma \eta^4(i e^\sigma)] \\ &= -\ln 2 - \sigma + \frac{\pi e^\sigma}{3} - 4 \sum_{n=1}^{\infty} \ln(1 - e^{-2n\pi e^\sigma}). \end{aligned} \quad (3)$$

This  $\xi(\sigma)$ , an even function of  $\sigma$ , has a global minimum at  $\sigma=0$  and increases exponentially as  $\sigma \rightarrow \pm\infty$ .  $\lambda_1$  is the 4-dimensional string coupling and takes a positive value.  $\lambda_2$  is proportional to the 4-dimensional trace anomaly of the  $N=2$  sector and determined by the number of chiral, vector, and spin- $\frac{3}{2}$  supermultiplets. It is important that  $\lambda_2$  can take positive values, since nonsingular solutions arise only when  $\lambda_2 > 0$ . In our simplified model (1), therefore, we assume  $\lambda$  to be positive (in actual numerical calculations we set  $\lambda = 1$ ) and adopt the form of the  $\xi$  function (3).

### A. Isotropic solutions

First, we review the homogeneous and isotropic case which is discussed in [4]. We neglect the spatial curvature and write the metric in the flat FRW form

$$ds^2 = -N(t)^2 dt^2 + a(t)^2 (dx^2 + dy^2 + dz^2). \quad (4)$$

Variation of the action (1) with respect to the lapse  $N$ , the scale factor  $a$ , and the modulus field  $\sigma$  gives three equations of motion as

$$\dot{\sigma}^2 = 6H^2 \left( 1 - \frac{\lambda}{2} H \xi \right), \quad (5)$$

$$(2\dot{H} + 5H^2) \left( 1 - \frac{\lambda}{2} H \xi \right) + H^2 \left( 1 - \frac{\lambda}{2} \dot{\xi} \right) = 0, \quad (6)$$

$$\ddot{\sigma} + 3H\dot{\sigma} + \frac{3\lambda}{2} (\dot{H} + H^2) H^2 \frac{\partial \xi}{\partial \sigma} = 0, \quad (7)$$

where  $H$  is the Hubble parameter  $\dot{a}/a$ , the overdot means derivative with respect to physical time  $t$ , and we have set  $N(t) = 1$ . As a result of the absence of scales [we are only

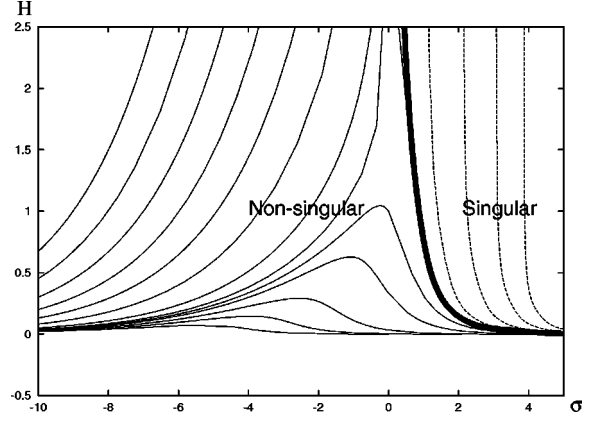


FIG. 1. The  $H$ - $\sigma$  phase diagram of isotropic solutions ( $\lambda = 1, H > 0, \dot{\sigma} > 0$ ). Time flows from left to right since  $\dot{\sigma} > 0$ . The nonsingular solutions are plotted with a solid line, and singular solutions with a dotted line. The bold line is a critical solution marking the border of singular and nonsingular solutions. All solution flows in the  $H > 0, \sigma < 0$  quarter-plane continue smoothly to the  $H > 0, \sigma > 0$  quarter-plane. In the  $H > 0, \sigma > 0$  quarter-plane, however, only the flows below the critical solution continue to the  $\sigma < 0$  region.

considering spatially flat metric (4)] and the existence of the constraint (5), the solutions are completely determined by a couple of first order differential equations for two variables  $H$  and  $\sigma$ ; that is, if we give values of  $H$  and  $\sigma$  at some time  $t$ , the preceding and following evolutions of the solution are automatically determined by these equations.

Figure 1 shows the  $H$ - $\sigma$  phase diagram of the isotropic system solved with initial conditions  $H > 0$  and  $\dot{\sigma} > 0$ . These solution flows are distinguished by only one degree of freedom (for example, the value of  $H$  at some fixed  $\sigma > 0$ ). There are singular solutions and nonsingular solutions, and it is shown in [4] that all flows in the  $H > 0, \sigma < 0$  quarter-plane continue smoothly to  $H > 0, \sigma > 0$  quarter-plane, but some flows in  $H > 0, \sigma > 0$  quarter-plane go into singularity and do not continue to the  $\sigma < 0$  region. It is also shown in [4] that the signs of  $H$  and  $\dot{\sigma}$  are conserved throughout the evolution of the system. Since  $\dot{\sigma}$  is always positive in Fig. 1, time flows from left to right. We consider that our Friedmann universe corresponds to the “future” region ( $\sigma > 0$ ) in Fig. 1, and we regard the “past” region ( $\sigma < 0$ ) with increasing Hubble parameter as a superinflation, which is expected to solve the shortcomings of the big-bang model.

### B. Equations of motion

We now extend the above model to anisotropic Bianchi type I space-time. We write the metric as

$$ds^2 = -N(t)^2 dt^2 + e^{2\alpha(t)} dx^2 + e^{2\beta(t)} dy^2 + e^{2\gamma(t)} dz^2, \quad (8)$$

and define the anisotropic expansion rates as

$$p = \dot{\alpha}, \quad q = \dot{\beta}, \quad r = \dot{\gamma}. \quad (9)$$

The average expansion rate, which coincides with the Hubble parameter  $H$  in the isotropic limit, is

$$H_{\text{avr}} = \frac{1}{3}(p+q+r). \quad (10)$$

The equations of motion are obtained by variation of the action (1) with respect to  $N, \alpha, \beta, \gamma$ , and  $\sigma$ , viz.,

$$pq+qr+rp - \frac{1}{2}\dot{\sigma}^2 - \frac{3}{2}\lambda \frac{\partial \xi}{\partial \sigma} \dot{\sigma} pqr = 0, \quad (11)$$

$$\dot{p} = \frac{(CA-EB)G + (EF-A^2)H + (AB-FC)Q}{\Delta}, \quad (12)$$

$$\dot{q} = \frac{(BC-DA)G + (BA-FC)H + (FD-B^2)Q}{\Delta}, \quad (13)$$

$$\dot{r} = \frac{(DE-C^2)G + (AC-BE)H + (BC-AD)Q}{\Delta}, \quad (14)$$

$$\begin{aligned} &\ddot{\sigma} + (p+q+r)\dot{\sigma} \\ &+ \frac{1}{2}\lambda \frac{\partial \xi}{\partial \sigma} \{\dot{p}qr + p\dot{q}r + pq\dot{r} + pqr(p+q+r)\} = 0, \end{aligned} \quad (15)$$

where

$$A = 1 - \frac{\lambda}{2} \frac{\partial \xi}{\partial \sigma} \dot{\sigma} p + \frac{\lambda^2}{4} \left( \frac{\partial \xi}{\partial \sigma} \right)^2 p^2 q r, \quad (16)$$

$$B = 1 - \frac{\lambda}{2} \frac{\partial \xi}{\partial \sigma} \dot{\sigma} q + \frac{\lambda^2}{4} \left( \frac{\partial \xi}{\partial \sigma} \right)^2 p q^2 r, \quad (17)$$

$$C = 1 - \frac{\lambda}{2} \frac{\partial \xi}{\partial \sigma} \dot{\sigma} r + \frac{\lambda^2}{4} \left( \frac{\partial \xi}{\partial \sigma} \right)^2 p q r^2, \quad (18)$$

$$D = \frac{\lambda^2}{4} \left( \frac{\partial \xi}{\partial \sigma} \right)^2 q^2 r^2, \quad (19)$$

$$E = \frac{\lambda^2}{4} \left( \frac{\partial \xi}{\partial \sigma} \right)^2 r^2 p^2, \quad (20)$$

$$F = \frac{\lambda^2}{4} \left( \frac{\partial \xi}{\partial \sigma} \right)^2 p^2 q^2, \quad (21)$$

$$\begin{aligned} G = &-p^2 - q^2 - pq - \frac{1}{2}\dot{\sigma}^2 + \frac{\lambda}{2} \frac{\partial^2 \xi}{\partial \sigma^2} \dot{\sigma}^2 p q \\ &- \frac{\lambda}{2} \frac{\partial \xi}{\partial \sigma} \dot{\sigma} p q r - \frac{\lambda}{4} \left( \frac{\partial \xi}{\partial \sigma} \right)^2 p^2 q^2 r (p+q+r), \end{aligned} \quad (22)$$

$$\begin{aligned} H = &-q^2 - r^2 - qr - \frac{1}{2}\dot{\sigma}^2 + \frac{\lambda}{2} \frac{\partial^2 \xi}{\partial \sigma^2} \dot{\sigma}^2 q r \\ &- \frac{\lambda}{2} \frac{\partial \xi}{\partial \sigma} \dot{\sigma} p q r - \frac{\lambda}{4} \left( \frac{\partial \xi}{\partial \sigma} \right)^2 p q^2 r^2 (p+q+r), \end{aligned} \quad (23)$$

$$\begin{aligned} Q = &-r^2 - p^2 - rp - \frac{1}{2}\dot{\sigma}^2 + \frac{\lambda}{2} \frac{\partial^2 \xi}{\partial \sigma^2} \dot{\sigma}^2 r p \\ &- \frac{\lambda}{2} \frac{\partial \xi}{\partial \sigma} \dot{\sigma} p q r - \frac{\lambda}{4} \left( \frac{\partial \xi}{\partial \sigma} \right)^2 p^2 q r^2 (p+q+r), \end{aligned} \quad (24)$$

and

$$\Delta = 2ABC + DEF - FC^2 - DA^2 - EB^2. \quad (25)$$

In the isotropic limit, Eqs. (11) and (15) become Eqs. (5) and (7), respectively, and Eqs. (12), (13), and (14) reduce to one equation (6). Similar to the isotropic case, once the values of  $\sigma, p, q$ , and  $r$  are given at some time  $t$ , and  $\dot{\sigma}$  is given according to the constraint (11), the system evolves along the flow of the solution following Eqs. (12)–(15). In our numerical analysis we integrated Eqs. (12)–(15) with the initial condition satisfying the constraint (11). This constraint equation (11) is also used to estimate the numerical error.

There are five parameters ( $\sigma, \dot{\sigma}, p, q$ , and  $r$ ) and one constraint (11); so the solution flows are drawn in a 4-dimensional space, for example,  $\sigma$ - $p$ - $q$ - $r$  space. Since the aim of this paper is to examine the effect of anisotropy on the nonsingular solution, we observe the change of the solution as we increase the anisotropy of the metric. To facilitate this we introduce two parameters indicating the anisotropy of the metric, viz.,

$$X = \frac{p-r}{p+q+r}, \quad Y = \frac{q-r}{p+q+r}. \quad (26)$$

In this notation,  $(X, Y) = (0, 0)$  corresponds to the isotropic (FRW) metric, and postulating  $H_{\text{avr}}$  to be positive, the region surrounded by the lines  $Y = 2X + 1, Y = \frac{1}{2}X - \frac{1}{2}, Y = -X + 1$  indicates the universe expanding in all directions (these lines are drawn in Figs. 3 and 6). The regions  $Y < 2X + 1, Y > \frac{1}{2}X - \frac{1}{2}, Y > -X + 1$ , etc., are the ‘‘Kasner-like’’ universe expanding in two directions and contracting in one direction. The regions  $Y > 2X + 1, Y > \frac{1}{2}X - \frac{1}{2}, Y > -X + 1$ , etc., describe the universe expanding in one direction, contracting in two directions. The universe shrinking in all directions cannot be included if we use Eqs. (26) and assume  $H_{\text{avr}} > 0$ . Instead of  $\sigma$ - $p$ - $q$ - $r$  we use  $\sigma$ - $H_{\text{avr}}$ - $X$ - $Y$  as four variables describing our system.

### C. Asymptotic solutions

Before going to the numerical analysis, we study the asymptotic form of the solutions at  $t \rightarrow \pm\infty, |\sigma| \rightarrow \infty$ . We assume  $|\sigma|$  to become large when  $t \rightarrow \pm\infty$ . The asymptotic form of the derivatives of the function  $\xi$  is

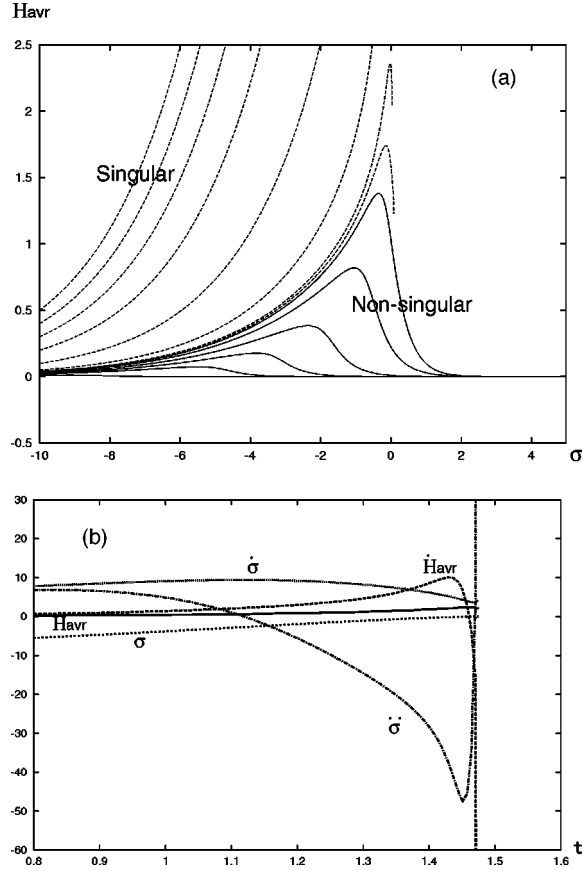


FIG. 2. (a) The average expansion rate in the anisotropic case. The equations are solved from  $\sigma = -10$ , where the initial anisotropy is fixed as  $X=0.1, Y=0.2$ . For large initial  $H_{\text{avr}}$ , there appear singularities with which the solution flows terminate suddenly, keeping  $H_{\text{avr}}$  and  $\sigma$  finite. (b) The behavior of  $H_{\text{avr}}$ ,  $\dot{H}_{\text{avr}}$ ,  $\sigma$ ,  $\dot{\sigma}$ , and  $\ddot{\sigma}$  in a singular solution appearing in (a). Initial conditions are the same as in (a) except the initial  $H_{\text{avr}}$  is set to 0.04. We can see  $\dot{H}_{\text{avr}}$  and  $\ddot{\sigma}$  diverge, but  $H_{\text{avr}}$ ,  $\sigma$ , and  $\dot{\sigma}$  stay finite.

$$\frac{\partial \xi}{\partial \sigma} \sim \text{sgn}(\sigma) \frac{\pi}{3} e^{|\sigma|}, \quad (27)$$

$$\frac{\partial^2 \xi}{\partial \sigma^2} \sim \frac{\pi}{3} e^{|\sigma|}. \quad (28)$$

If we assume the power-law ansatz for the expansion rates, the asymptotic form of the modulus has to be logarithmic in order to cancel the exponential dependence of Eqs. (27) and (28). Thus we choose the following forms for the asymptotic solutions:

$$p \sim \omega_1 |t|^\rho, \quad (29)$$

$$q \sim \omega_2 |t|^\rho, \quad (30)$$

$$r \sim \omega_3 |t|^\rho, \quad (31)$$

$$\sigma \sim \sigma_0 + \omega_4 \ln|t|. \quad (32)$$

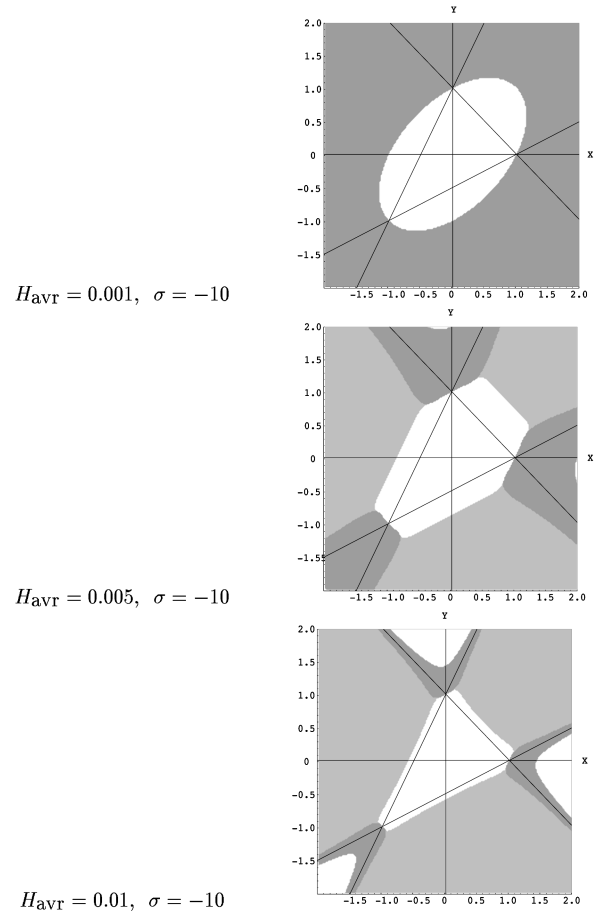


FIG. 3. Constraint and  $\Delta$  on the  $\sigma = -10$  section of the  $X$ - $Y$  plane.  $H_{\text{avr}}$  is 0.001, 0.005, 0.01 from above.  $\Delta > 0, \Delta < 0$ , and excluded regions are indicated by white, light-shaded, and dark-shaded areas, respectively. In the dark gray region the Hamiltonian constraint (11) is not satisfied, and  $\Delta$  cannot be defined. Cosmological solutions inhabit the white and light gray regions, and those in each region are separated by singularities since  $p, q, r$  become infinite when  $\Delta = 0$  [see Eqs. (12), (13), and (14)].

Putting all these into Eqs. (11)–(15), we obtain two possible asymptotic solutions:

$$\mathcal{A}: \rho = -1, \omega_1 + \omega_2 + \omega_3 = \text{sgn}(t),$$

$$\omega_1^2 + \omega_2^2 + \omega_3^2 + \omega_4^2 = 1, \quad (33)$$

$$\mathcal{B}: \rho = -2, |\omega_4| = 5,$$

$$\omega_1 \omega_2 \omega_3 = -\text{sgn}(t) \frac{5 \exp[-\sigma_0 \text{sgn}(\omega_4)]}{\lambda \pi}. \quad (34)$$

The solution  $\mathcal{A}$  is obtained by balancing terms that do not include the 1-loop effect, i.e., the Gauss-Bonnet term, and thus describes the asymptotic behavior where the Gauss-Bonnet effect is negligible. In the absence of the modulus field,  $\mathcal{A}$  is nothing but the Bianchi type I vacuum (Kasner) solution. The solution  $\mathcal{B}$  is obtained by balancing the kinetic term of the modulus and the Gauss-Bonnet term, and this

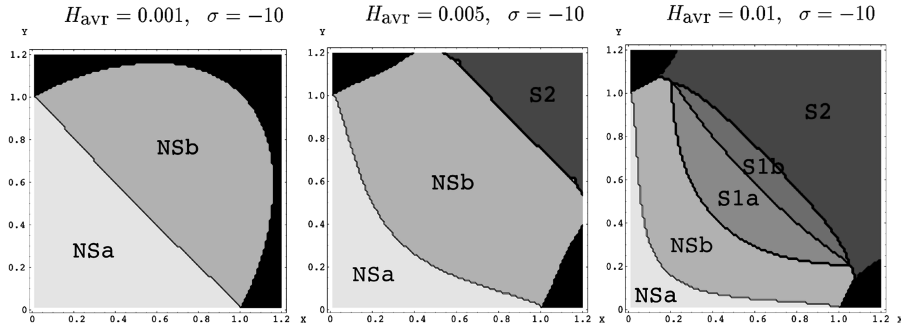


FIG. 4. Solutions through the  $\sigma = -10$  cross section.  $H_{avr}$  is 0.001, 0.005, 0.01 from the left. NS means nonsingular. NSa leads to a Friedmann-type solution (expanding in all directions) and NSb leads to a Kasner-type solution (expanding in two directions and shrinking in one direction) in the future asymptotic region. S1 means it leads to a singularity where  $\Delta \rightarrow 0$ . S1a is the solution whose behavior near such a singularity is  $p\dot{p} > 0, q\dot{q} > 0, r\dot{r} > 0$ , while S1b behaves as  $p\dot{p} < 0, q\dot{q} < 0, r\dot{r} < 0$ , near the singularity. S2 leads to a singularity where  $\Delta \rightarrow -\infty$ .

solution corresponds to the phase where the Gauss-Bonnet term is important. Other possibilities of solutions are excluded as long as we impose  $\lambda > 0$ , which is, in the isotropic limit, a necessary condition for the existence of the nonsingular solutions.

Following the isotropic case [3–5], we choose  $\dot{\sigma} > 0$  and assume the solution  $\mathcal{A}$  in the future asymptotic region and  $\mathcal{B}$

in the past asymptotic region. Then, in the region  $t \rightarrow \infty$ , the conditions (33) can be seen in the  $\omega_1 - \omega_2 - \omega_3$  space as the cross section of the sphere of radius  $\sqrt{1 - \omega_4^2}$  centered at the origin with the  $\omega_1 + \omega_2 + \omega_3 = 1$  plane. Depending on the asymptotic value of  $\omega_4$ , the asymptotic solutions of  $t \rightarrow \infty$  are categorized into two cases.

$\mathcal{A}1: 0 \leq \omega_4 < \frac{1}{\sqrt{2}}$ . The asymptotic solution is either ex-

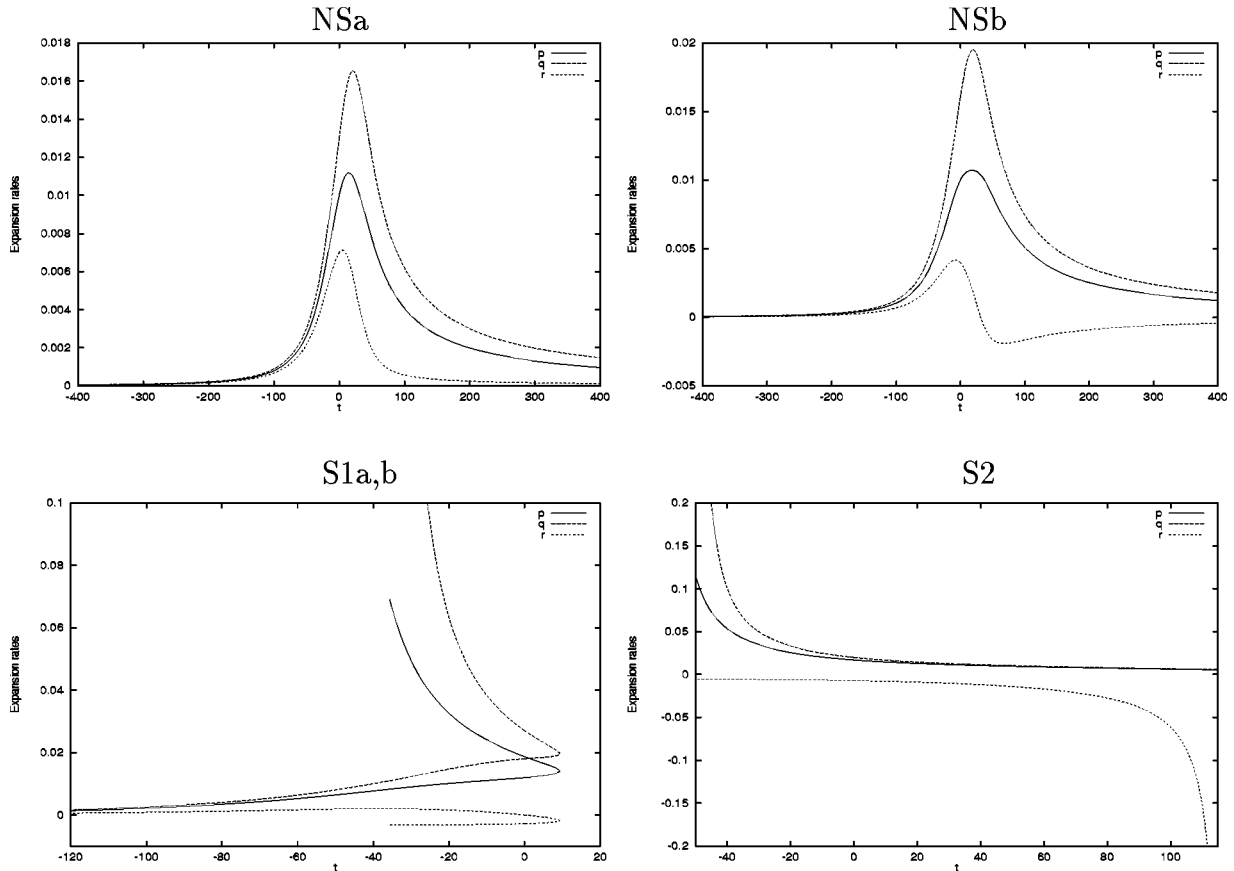


FIG. 5. Behavior of solutions appearing in Fig. 4.  $t = 0$  is the time when  $\sigma = -10$ . These are solutions through the points  $(X, Y) = (0.1, 0.2), (0.2, 0.4), (0.4, 0.6)$ , and  $(0.8, 0.9)$ , respectively, in the  $H_{avr} = 0.01, \sigma = -10$  plane.

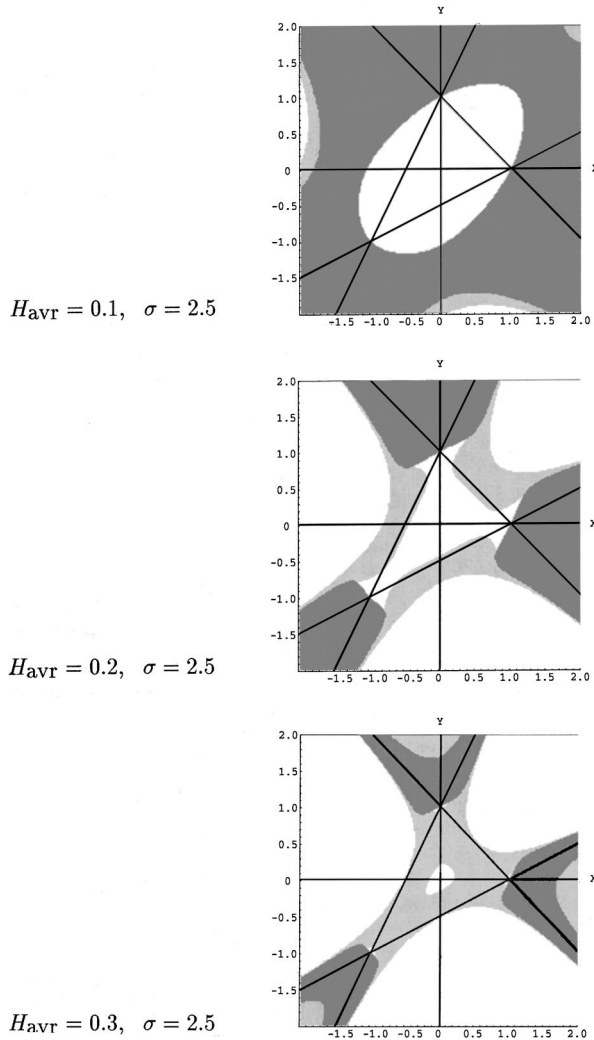


FIG. 6. Constraint and  $\Delta$  on the  $\sigma=2.5$  section of the  $X$ - $Y$  plane.  $H_{\text{avr}}$  is 0.1, 0.2, 0.3 from above.  $\Delta > 0, \Delta < 0$ , and excluded regions are indicated by white, light-shaded, and dark-shaded areas, respectively.

panding in all directions (Friedmann type) or expanding in two directions, shrinking in one direction (Kasner type).

$\mathcal{A}2: \sqrt{\frac{1}{2}} \leq \omega_4 \leq \sqrt{\frac{2}{3}}$ . The asymptotic solution is Friedmann type only.

In terms of  $X$  and  $Y$  introduced in Eq. (26), the asymptotic solution is represented by a point on an arc of the ellipse  $X^2 + Y^2 - XY = 1 - \frac{3}{2}\omega_4^2$ . Thus  $\mathcal{A}2$  falls into the region inside the oval  $X^2 + Y^2 - XY = \frac{1}{4}$ , and  $\mathcal{A}1$  is in the region between two ellipses  $X^2 + Y^2 - XY = \frac{1}{4}$  and  $X^2 + Y^2 - XY = 1$ . No asymptotic solutions exist in the region outside the ellipse  $X^2 + Y^2 - XY = 1$ , where the constraint equation (11) is not satisfied. Therefore, at least in the far enough future region, it is sufficient to examine solutions near the isotropic one. The difference in our model from the Kasner (Bianchi type I vacuum) solution is the existence of the field  $\sigma$ , which allows the existence of a Friedmann-type solution in the future asymptotic region.

In the past asymptotic region, the condition (34) indicates  $\omega_1 \omega_2 \omega_3 > 0$ , i.e. one of the following.

$\mathcal{B}1: \omega_1, \omega_2, \omega_3 > 0$ .

$\mathcal{B}2$ : One of  $\omega_i (i=1,2,3)$  is positive; two are negative.

This means that in the past asymptotic region the universe is either expanding in all directions or expanding in one direction contracting in two directions.

### III. NUMERICAL RESULTS

Once the anisotropy is included, the behavior of the solution deviates substantially from the isotropic case. Figure 2a shows the average expansion rate  $H_{\text{avr}} = (p+q+r)/3$  versus the modulus  $\sigma$  in the anisotropic (Bianchi type I) case, solved with initial anisotropy  $X=0.1, Y=0.2$  at  $\sigma=-10$ . Unlike the isotropic case (Fig. 1), some solution flows in the  $\sigma < 0$  region do not continue smoothly to the  $\sigma > 0$  region, but terminate suddenly with finite values of  $\sigma$  and  $H_{\text{avr}}$ . At these unusual singularities the time derivatives of  $p, q$ , and  $r$  become infinite, although  $p, q$ , and  $r$  themselves stay finite (see Fig. 2b). This is because the value of  $\Delta$ , Eq. (25), approaches zero, while the numerators of Eqs. (12), (13), and (14) stay finite. Thus, the function  $\Delta$  plays an important role in the anisotropic case, and the regularity of the solutions depends largely on its behavior.

In the equations in our model there are four independent variables  $\sigma-H_{\text{avr}}-X-Y$ . Since our interest is mainly in the vicinity of the isotropic solution, we examine the solutions which pass near the origin of the  $X$ - $Y$  plane, first at the  $\sigma = -10$  section with several different values of  $H_{\text{avr}}$  and next at the  $\sigma = 2.5$  section.

#### A. Solutions through the $\sigma = -10$ cross section

It is helpful to consider the general behavior of  $\Delta$  and the region prohibited by the constraint equation before solving the equations numerically. Rewriting  $\Delta$ , Eq. (25), and the constraint equation (11) in terms of  $\sigma, H_{\text{avr}}, X$ , and  $Y$ , we can specify  $\Delta > 0, \Delta < 0$ , and prohibited regions on the  $X$ - $Y$  plane for fixed  $\sigma$  and  $H_{\text{avr}}$ , which is shown in Fig. 3. The dark-shaded region is the prohibited region, the light-shaded region is where  $\Delta < 0$ , and the white region is where  $\Delta > 0$ . Since  $\Delta = 0$  is not physically allowed [ $\dot{p}, \dot{q}$  and  $\dot{r}$  diverge from Eqs. (12), (13), and (14)], the solutions in the white region cannot go smoothly to the light-shaded region. Also indicated in Fig. 3 are the lines  $X+Y=1$ , etc., discussed in Sec. II B. We can see that the universe expanding in all directions always lies in the  $\Delta > 0$  region. For larger  $H_{\text{avr}}$  the prohibited region becomes thinner, and the white and light gray regions will be separated by the lines  $X+Y=1$ , etc.

Starting from the initial conditions  $\sigma = -10$  and  $H_{\text{avr}} = 0.001, 0.005, 0.01$ , we solved the equations futureward and indicated the behavior of the solutions in the  $X$ - $Y$  plane (Fig. 4). Because of the symmetry of the axes, we restrict the region to  $X > 0, Y > 0$ , and since we are not interested in the prohibited region, we only examined the vicinity of the origin.

The black region in Fig. 4 is prohibited by the Hamiltonian constraint, and the regions marked NS means nonsingular solutions. The difference between NSa and NSb is in their form in the future asymptotic region, where NSa has

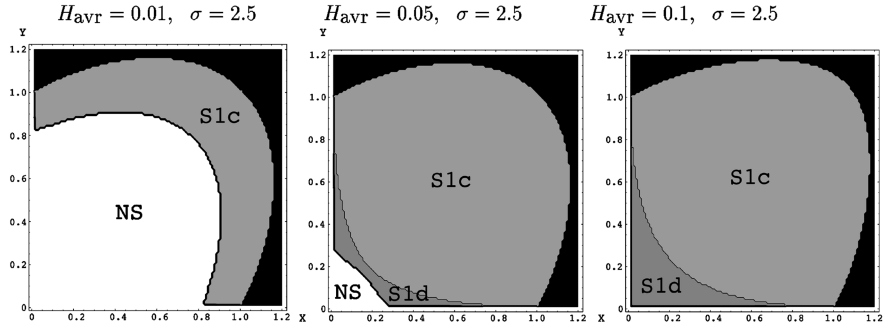


FIG. 7. Solutions through the  $\sigma=2.5$  cross section.  $H_{\text{avr}}$  is 0.01, 0.05, 0.1 from the left. NS means nonsingular, which leads to an expanding universe in the past asymptotic region. S1 means it leads to a singularity where  $\Delta \rightarrow 0$ . S1c is the solution whose behavior near such a singularity is  $p > 0, q > 0, r < 0$ , while S1d behaves as  $p > 0, q > 0, r > 0$ , near the singularity.

Friedmann-type (expanding in all directions) and NSb has Kasner-type (expanding in two directions and contracting in one direction) asymptotic solutions. Examples of NSa and NSb solutions are shown in the first and the second panels of Fig. 5. The solutions in the region marked S1 in Fig. 4 lead to singularities where  $\Delta \rightarrow 0$  (we term this singularity type I) and these singular solutions are the same as those appearing in Fig. 2. We divided the S1 solutions into two classes, S1a and S1b. S1a approaches the singularity as  $p\dot{p} > 0, q\dot{q} > 0, r\dot{r} > 0$ , while S1b as  $p\dot{p} < 0, q\dot{q} < 0, r\dot{r} < 0$ . This singularity, since it arises because  $\Delta$  crosses zero, can be overpassed if we introduce a new “time” variable

$$d\tau = dt/\Delta. \quad (35)$$

Using this  $\tau$ , two solutions S1a and S1b can be joined via the singularity, which is shown in the third panel of the Fig. 5 (S1a,b). The solution S1b, solved backwards in time, goes into another singularity which has different property from the one between S1a and S1b. At this singularity, which we call type II,  $\Delta$  goes to  $-\infty$ , and at least one of the expansion rates ( $q$  in the case of Fig. 5, S1a,b) diverges. We can say that this solution (S1a and S1b joined together) comes regularly from  $t = -\infty$ , turns back at type I singularity, and then goes backwards in time into a type II singularity. Or we can also see this as two solutions, one coming from  $t = -\infty$  and the other from the type II singularity, “pair-annihilate” at one type I singularity. S2 is yet another solution, which comes from one type II singularity and disappears into another type II singularity. As  $H_{\text{avr}}$  becomes larger, the boundary between S1a and S1b ( $\Delta = 0$  line in Fig. 3) gets pushed to approach the line  $X + Y = 1$ , and accordingly the nonsingular regions NSa and NSb become smaller. This is consistent with Fig. 2, which shows the existence of the upper limit of  $H_{\text{avr}}$  for the regular solution through the  $\sigma < 0$  region.

### B. Solutions through the $\sigma=2.5$ cross section

As is expected from the isotropic case discussed in the previous section, the solutions through the  $\sigma > 0$  cross section are quite different from those through the  $\sigma < 0$  section. In Fig. 6 we show the prohibited region (dark shaded),  $\Delta > 0$  region (white), and  $\Delta < 0$  region (light shaded) in the  $X$ - $Y$  plane, with  $\sigma$  fixed to 2.5. The elliptic allowed region of

small  $H_{\text{avr}}$  is the one discussed in relation to the future asymptotic form of the solution, which is expressed as  $X^2 + Y^2 - XY = 1$ . As  $H_{\text{avr}}$  takes large values the  $\Delta = 0$  contour takes complicated forms, and the region connected to the isotropic solution becomes small.

Figure 7 shows the solutions passing through the  $X$ - $Y$  plane of the  $\sigma=2.5$  cross section, and the time evolution of each type is shown in Fig. 8.  $H_{\text{avr}}$  is chosen to be 0.01, 0.05, and 0.1. As  $H_{\text{avr}}$  increases the nonsingular region becomes smaller, and for  $H_{\text{avr}}$  larger than 0.1 the nonsingular solution completely disappears from the  $X$ - $Y$  plane. All the singularities appearing in Fig. 7 are type I, and these singular solutions can be extended further by using  $\tau$  defined by Eq. (35). Just like the S1a and S1b solutions in the previous subsection, S1c and S1d, extended beyond the type I singularity, turn back futurewards and then go into the type II singularity. The only difference between these and S1a,b is the direction of time, and the former can be regarded as the “pair creation” of cosmological solutions, while the latter is the “pair annihilation.”

One of the nontrivial results of our analysis, and what makes this model very different from ordinary universe models, is that the “initial singularity” in the isotropic limit is categorized into the type I singularity (see the third panel of Fig. 7 and compare S1d and isotropic solutions in Fig. 8). This means that the singular solutions in the model proposed by Antoniadis, Rizos, and Tamvakis [3] or Rizos and Tamvakis [4] will, if small anisotropy is included, terminate suddenly at finite past with finite Hubble parameter or, if extended using  $\tau$ , turn back towards the future.

All nonsingular solutions in Figs. 7 and 8 continue to the asymptotic solutions expanding in all directions in the past asymptotic region. That is, the asymptotic form  $\mathcal{B}1$  (discussed in Sec. II C) can be reached from  $\sigma=2.5$  but  $\mathcal{B}2$  cannot. There exist solutions having the past asymptotic form  $\mathcal{B}2$ . For example, solutions through the outer white ( $\Delta > 0$ ) region in the third panel of Fig. 3 behave as  $\mathcal{B}2$  in the  $t \rightarrow -\infty$  region. These solutions, however, go into singularities between  $\sigma = -10$  and  $\sigma = 2.5$ , and do not appear in Fig. 7 or 8.

### C. Nature of the singularity

In our numerical analysis there appear two types of singularities, which we called type I and type II. We discuss the nature of these singularities briefly.

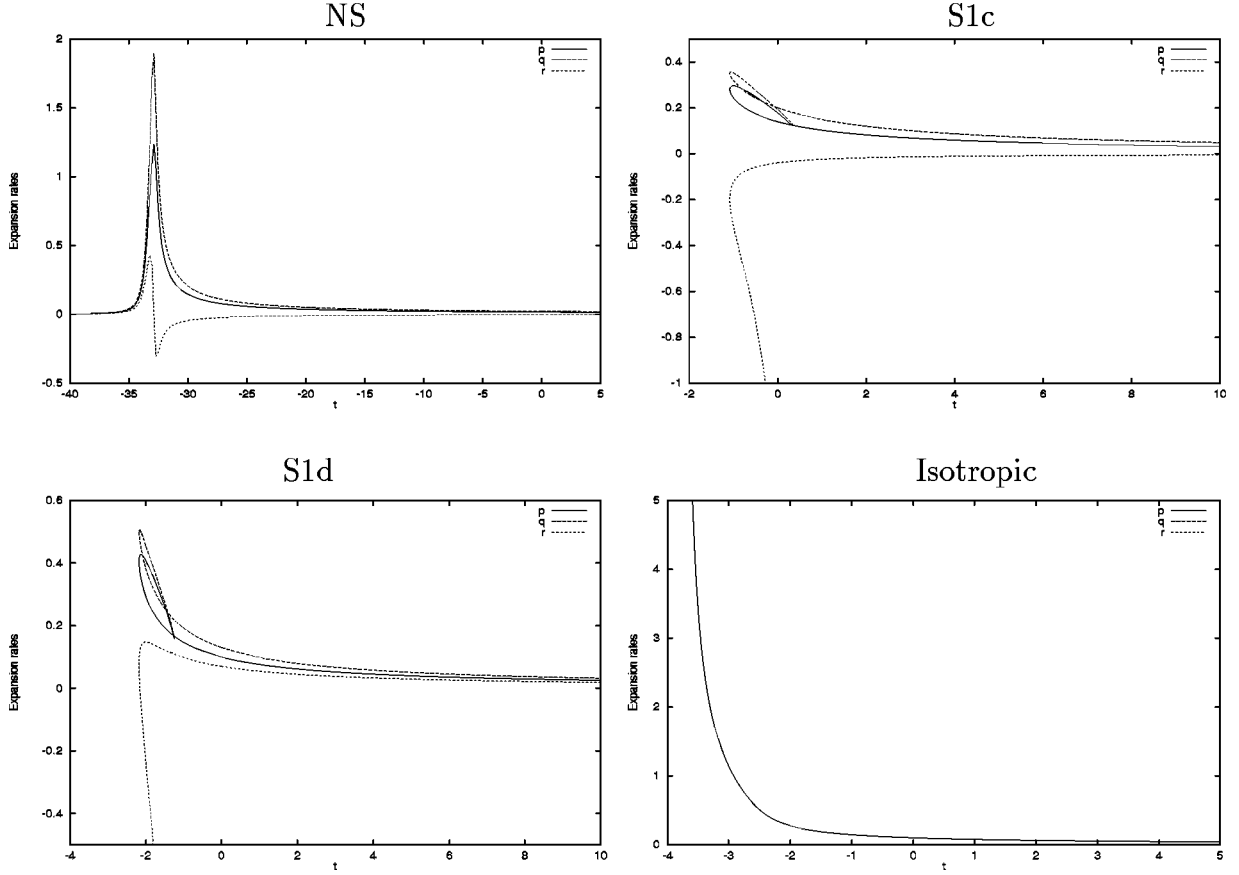


FIG. 8. Behavior of solutions appearing in Fig. 7.  $t=0$  is the time when  $\sigma=2.5$ . The initial values are chosen on the  $\sigma=2.5$  plane as  $(H_{\text{avr}}, X, Y) = (0.01, 0.6, 0.8), (0.1, 0.6, 0.8), (0.1, 0.1, 0.2)$ , and  $(0.1, 0.0, 0.0)$  for NS, S1c, S1d, and isotropic examples of the solution, respectively.

At type I singularities the expansion rates  $(p, q, r)$  stay finite whereas the time derivatives of them diverge. These situations happen when  $p, q, r \sim |t - t_{\text{sing}}|^\rho$  with  $0 < \rho < 1$ . This is actually the case, and can be verified by analyzing solutions near the singularity. Although the type I singularity ( $\Delta=0$ ) is a physical one, the equations of motions can be integrated regularly by using the new “time” parameter  $\tau$ , Eq. (35), through the type I singularity. At the singularity  $p, q, r$  “turn around” (see the solutions S1 in Figs. 5 and 8), meaning that  $p, q$ , and  $r$  are multiple-valued function of  $t$ . Since  $dt = \Delta d\tau = 0$  at the singularity, the solutions are tangential to  $t = t_{\text{sing}}$ . Also, in order that the solutions change the chronological direction, the leading power of  $p, q, r$  in the expansion of  $t$  near the singularity must be even. Thus we can express  $t$  using  $p, q, r$  as

$$\begin{aligned}
 t - t_{\text{sing}} &= t_{p,2l}(p - p_{\text{sing}})^{2l} + t_{p,2l+1}(p - p_{\text{sing}})^{2l+1} + \dots \\
 &= t_{q,2m}(q - q_{\text{sing}})^{2m} + t_{q,2m+1}(q - q_{\text{sing}})^{2m+1} + \dots \\
 &= t_{r,2n}(r - r_{\text{sing}})^{2n} + t_{r,2n+1}(r - r_{\text{sing}})^{2n+1} + \dots, \quad (36)
 \end{aligned}$$

with  $l, m, n$  being positive integers. By solving these with respect to  $p, q$ , and  $r$ , we have

$$p = p_{\text{sing}} + p_1(t - t_{\text{sing}})^{1/2l} + \dots, \quad (37)$$

$$q = q_{\text{sing}} + q_1(t - t_{\text{sing}})^{1/2m} + \dots, \quad (38)$$

$$r = r_{\text{sing}} + r_1(t - t_{\text{sing}})^{1/2n} + \dots. \quad (39)$$

Thus,  $0 < 1/2l, 1/2m, 1/2n < 1$ , and  $\dot{p} = (p_1/2l)(t - t_{\text{sing}})^{1/2l-1} + \dots$ , etc., will diverge. The behavior of  $\dot{\sigma}$  is similar to that of  $p, q$ , and  $r$ . In our numerical calculations (S1 of Figs. 5 and 8),  $l, m, n$  take the values  $l = m = n = 1$ , which is the most generic case.

In the vicinity of other types of singularities, analytic expressions of the solutions are obtained by assuming power-law behavior of the scale factors and the regularity of the modulus field, just as in the isotropic case [3]. Because of the anisotropy, there are 3 cases of singular solutions other than the type I:

$$C1: p \sim p_1/t, q \sim q_0, r \sim r_0, \sigma \sim \sigma_0, \dot{\sigma} \sim \sigma_1, \ddot{\sigma} \sim \sigma_2,$$

$$p_1 = 1, q_0 + r_0 - \frac{3}{2}\lambda \frac{\partial \xi}{\partial \sigma} \Big|_{\sigma_0} \sigma_1 q_0 r_0 = 0, \quad (40)$$

$$C2: p \sim p_1/t, q \sim q_1/t, r \sim r_0, \sigma \sim \sigma_0, \dot{\sigma} \sim \sigma_1, \ddot{\sigma} \sim \sigma_2,$$

$$p_1 = q_1 = 1, 1 - \frac{3}{2} \lambda \frac{\partial \xi}{\partial \sigma} \Big|_{\sigma_0} \sigma_1 r_0 = 0, \quad (41)$$

$$C3: p \sim p_1/t, q \sim q_1/t, r \sim r_1/t, \sigma \sim \sigma_0, \dot{\sigma} \sim \sigma_1 t, \ddot{\sigma} \sim \sigma_1,$$

$$p_1 = q_1 = r_1 = 1, 1 - \frac{1}{2} \lambda \frac{\partial \xi}{\partial \sigma} \Big|_{\sigma_0} \sigma_1 = 0, \quad (42)$$

where we have chosen the origin of  $t$  at the singularity.  $C1$  is the case where only one of the three expansion rates ( $p, q, r$ ) is singular,  $C2$  two, and  $C3$  all three. The solution  $C1$  agrees well with our numerical results (S2 of Fig. 5). Since  $p_1, q_1, r_1 = 1$  (if not zero), the divergent behavior is determined by the sign of  $t$ ; i.e., if a solution goes into a singularity futureward ( $t \rightarrow -0$ ), then  $p \rightarrow -\infty$ , etc., and if pastward ( $t \rightarrow +0$ ),  $p \rightarrow +\infty$ , etc. Putting Eqs. (40)–(42) into Eq. (25), we have  $\Delta \rightarrow -\infty$  for  $C1$  and  $C2$  but  $\Delta \rightarrow +0$  for  $C3$ . Therefore, according to our definition of the singularities ( $\Delta \rightarrow 0$  for type I and  $\Delta \rightarrow -\infty$  for type II),  $C1$  and  $C2$  will be categorized into type II and  $C3$  will be categorized into type I. In the isotropic case ( $p = q = r$ ), we can show that  $\Delta > 0$  is always satisfied, and  $C3$  can be seen as a type I singularity ‘‘pushed towards the infinity.’’

All of these singularities, both types I and II, are physical singularities. This can be shown by putting  $p, q, r$  and  $\dot{p}, \dot{q}, \dot{r}$  into the curvature scalar  $R = 2(\dot{p} + p^2 + \dot{q} + q^2 + \dot{r} + r^2 + pq + qr + rp)$ .

#### D. Summary of numerical results

We extended the nonsingular universe model proposed by Rizos and Tamvakis [4] to include anisotropy, and examined solutions in the vicinity of the isotropic solution in both  $\sigma < 0$  and  $\sigma > 0$  regions. We found both nonsingular solutions and singular solutions. Nonsingular solutions inhabit the region where the anisotropy is small, and they evolve from the past asymptotic region, superinflate, and then lead either to Friedmann-type or to Kasner-type solutions in the future. Singularities appearing in our analysis are classified into two types, namely, type I and type II. The type I singularity corresponds to the crossing of  $\Delta = 0$ , and  $\dot{p}, \dot{q}$ , and  $\dot{r}$  diverge, while  $p, q, r$ , and  $\sigma, \dot{\sigma}$  stay finite. At the type II singularity, on the other hand,  $\Delta$  tends to  $-\infty$ , and  $p, q$  and  $r$  will diverge. The evolution of the singular solutions is characterized by the behavior of  $\Delta$ . At the origin of the  $X$ - $Y$  plane (isotropic solution)  $\Delta$  is always positive regardless of the values of  $\sigma$  or  $H_{\text{avr}}$ , and as anisotropy increases there appear  $\Delta < 0$  regions or regions prohibited by the constraint equation (11), which is shown in Figs. 3 and 6. There are three types of singular solutions appearing in our analysis (if two branches connected by a type I singularity are counted as one solution). The first type of singular solution is marked by the crossing of the  $\Delta = 0$  line, which we termed the type I singularity, in the future. This includes S1a and S1b in Figs. 4 and 5, and if we continue the solution beyond  $\Delta = 0$  by changing the variable, this singular solution can be seen as a pair annihilation of the  $\Delta > 0$  and  $\Delta < 0$  branches of solutions. The  $\Delta > 0$  branch continues from the infinite past,

while the  $\Delta < 0$  branch leads to a type II singularity at the finite past. The second singular solution is very similar to the first one, except it crosses the  $\Delta = 0$  line in the past. This solution, examples of which are S1c and S1d of Figs. 7 and 8, can be regarded as a pair creation of two branches. The singular solution in the isotropic model [3,4] is a special case of this second singular solution. The third singular solution lies always in the  $\Delta < 0$  region and never crosses the  $\Delta = 0$  line, i.e., includes no type I singularity. This solution is born in the type II singularity, and disappears into the type II singularity (see S2 of Fig. 4 and 5).

#### IV. CONCLUSION

In this paper we presented anisotropic nonsingular cosmological solutions derived from the 1-loop effective action of the heterotic string. We found nonsingular solutions which evolve from the infinite past asymptotic region, superinflate, and then continue either to Friedmann-type or Kasner-type solutions. The singular solutions of moderate anisotropy are classified into three types, and involved in these solutions are two types of singularities: one corresponds to  $\Delta = 0$  and the other to  $\Delta = -\infty$ . The initial singularity in the isotropic limit is a special case of the  $\Delta = 0$  singularity.

Violation of the energy conditions, which is necessary to avoid the singularity, is achieved by the existence of a Gauss-Bonnet term coupled to a modulus field. This can be confirmed by using the asymptotic forms (33) and (34) for nonsingular solutions. We define the effective energy density and effective pressure as

$$\epsilon := -G^0_0 = pq + qr + rp, \quad (43)$$

$$p_1 := G^1_1 = -(\dot{q} + \dot{r} + q^2 + r^2 + qr), \quad (44)$$

$$p_2 := G^2_2 = -(\dot{r} + \dot{p} + r^2 + p^2 + rp), \quad (45)$$

$$p_3 := G^3_3 = -(\dot{p} + \dot{q} + p^2 + q^2 + pq). \quad (46)$$

Assuming the asymptotic solution  $\mathcal{A}$  in the region  $t \rightarrow \infty$  and that  $\dot{\sigma}$  is always positive (in our numerical analysis  $\dot{\sigma}$  keeps its sign except the singular solution S2), the effective energy density and pressure behave in the future asymptotic region as  $\epsilon, p_i \sim \frac{1}{2} \omega_4^2 |t|^{-2}$  ( $i = 1, 2, 3$ ). Thus, the weak energy condition  $\epsilon + p_i \sim \omega_4^2 |t|^{-2} > 0$  and the strong energy condition  $\epsilon + \sum p_i \sim 2\omega_4^2 |t|^{-2} > 0$  are satisfied. In the past asymptotic region, on the other hand, the asymptotic solution becomes  $\mathcal{B}$  in which the Gauss-Bonnet term is dominant. Then  $\epsilon \sim (\omega_1 \omega_2 + \omega_2 \omega_3 + \omega_3 \omega_1) |t|^{-4}$  and  $p_1 \sim -2(\omega_2 + \omega_3) |t|^{-3} - (\omega_2^2 + \omega_3^2 + \omega_2 \omega_3) |t|^{-4}$ , etc. If the weak energy condition is satisfied,  $\epsilon + p_i > 0$  for  $i = 1, 2, 3$ , and so  $3\epsilon + \sum p_i \sim -4(\omega_1 + \omega_2 + \omega_3) |t|^{-3}$  must be positive. If the strong energy condition is satisfied,  $\epsilon + \sum p_i \sim -4(\omega_1 + \omega_2 + \omega_3) |t|^{-3}$  must be positive. Neither of them is possible as

long as  $H_{\text{avr}} \sim (\omega_1 + \omega_2 + \omega_3) |t|^{-2/3} > 0$ . Therefore, weak and strong energy conditions are violated in the past asymptotic region.

One of the biggest advantages of our model is that it includes a rather long period of (super) inflationary stage in a natural form. However, our result, which admits the evolution of an almost-isotropic superinflating solution into a Kasner-type anisotropic solution (see the panel ‘‘NSb’’ of Fig. 5, for example), suggests that the superinflation in our model does not isotropize the space-time. Our recent study [7] of the cosmological perturbation for the homogeneous

and isotropic background shows the existence of exponential growth in graviton-mode perturbation during the superinflationary stage. Together with this we can conclude that the cosmic no-hair hypothesis [8] does not hold in this superinflationary model. We are interested in whether this result is common to all kinetic-driven superinflation.

#### ACKNOWLEDGMENTS

This work of J.S. is supported by Grant-in-Aid for Scientific Research No. 10740118.

- 
- [1] M. Gasperini and G. Veneziano, *Astropart. Phys.* **1**, 317 (1993); *Mod. Phys. Lett. A* **8**, 3701 (1993); *Phys. Rev. D* **50**, 2519 (1994).
- [2] R. Brustein and G. Veneziano, *Phys. Lett. B* **329**, 429 (1994); N. Kaloper, R. Madden, and K.A. Olive, *Nucl. Phys.* **B452**, 677 (1995); M. Gasperini, M. Maggiore, and G. Veneziano, *ibid.* **B494**, 315 (1997); R. Brustein and R. Madden, *Phys. Lett. B* **410**, 110 (1997).
- [3] I. Antoniadis, J. Rizos, and K. Tamvakis, *Nucl. Phys.* **B415**, 497 (1994).
- [4] J. Rizos and K. Tamvakis, *Phys. Lett. B* **326**, 57 (1994).
- [5] R. Easther and K. Maeda, *Phys. Rev. D* **54**, 7252 (1996).
- [6] J.A. Harvey and G. Moore, *Phys. Rev. D* **57**, 2323 (1998).
- [7] S. Kawai, M. Sakagami, and J. Soda, *Phys. Lett. B* **437**, 284 (1998).
- [8] R. Wald, *Phys. Rev. D* **28**, 2118 (1983); M.S. Turner and L.M. Widrow, *Phys. Rev. Lett.* **57**, 2237 (1986); L.G. Jensen and J.A. Stein-Schabes, *Phys. Rev. D* **34**, 931 (1986).